Transfer Report

Identification of Vertebra Characteristics that Determine Different Mechanical Outcomes of Vertebroplasty

Gavin Day

Supervisors: Professor Ruth Wilcox & Dr Alison Jones

University of Leeds

June 23, 2017

Contents

List of Figures

List of Tables

Chapter 1

Human Tissue

1.1 Introduction

1.2 Methods

1.2.1 Potting

The geometry of human lumbar vertebrae varies considerably to that of the bovine tail vertebrae from which this methodology is based. This is characterised by much larger posterior elements with the facets extending much lower, below the bottom of the vertebral body. Hence, to correctly pot the human vertebrae much more cement must be used, especially for the posterior end-cap, in order to cover the bottom of the vertebral body and the extending posterior elements. This means that much more of the posterior elements are constrained, therefore restricting the rotation of the vertebral body endplates under axial load. In addition to this the larger posterior elements which are captured within the PMMA end-caps will transmit load and take a greater share of the load when compared to the bovine tail vertebrae. Given that vertebroplasty attempts to restore the stiffness of the vertebral body and that there is no understanding of specifically how the loads are shared between the vertebral body and posterior element, this presents a problem.

A solution to this is to remove the posterior elements, following such methods as [41, 59], where only the vertebral body is modelled. This allows the stiffness of the vertebral body alone to be captured and modelled. The posterior elements were removed by cutting through the pedicles at the narrowest part, limiting damage to the region.

To pot the specimens that now lack a spinal canal, a retort stand was used to hold the vertebra, ensuring that both endplates were level on average. The specimen was then lowered down into the potting container leaving 5 mm between the bottom of the vertebra and the container. PMMA was poured into the container until the entire of the endplate was touching cement, with the edges of the vertebral body covered. Care needed to be taken to ensure all of the endplate was in contact with cement, given the extent of osteophytes creating non-flat surfaces in some of the more degenerated specimens. The other side of the vertebra was potted in a similar manner, however, due to the constraints of the potting container a measured quantity of cement was poured prior to lowering the vertebra into it. A spirit level ensured parallel end-caps.

1.2.2 Loading

Following previous studies [41], the vertebrae were loaded with an initial maximum load of 800 N for similarly osteoporotic vertebrae. However, after loading two of the initial set of vertebrae the stiffness continued to increase up to maximum 800 N. Following loads up to 2000 N showed that the stiffness reached a maximum between 1300 and 2000 N, with three of the initial four specimens showing some degree of failure in the final 400 N of loading.

1.2.2.1 Maximum Stiffness Measurement

The maximum stiffness of the vertebra was found in the same fashion as with the bovine tail vertebrae - measuring the stiffness of segments at increments over the length of the curve. Given that damage, especially for the intact specimens, needs to be avoided the maximum loads used are on the conservative side. This can mean that the maximum stiffness is potentially at the end of the data set or that the stiffness is still increasing at the load cut off. The solution to the latter would require a prediction of the yield point prior to experimental loading (discussed in Section 1.2.5.2), while the former could potentially be solved by using smaller segment sizes when measuring the stiffness from load - displacement results.

To allow the effect of segment size (the length of each section from which the stiffness is found) and increment size (the size of each increment defining the start point of each segment), the maximum stiffness finding Matlab code was rewritten in Python. This function could then be iterated over, reporting the maximum stiffness when using an increment size of between 1 and 100 data points (the distance between two data points corresponds to 0.0017 mm). Changing the increment size becomes a verification of the results using an increment size of 1 data point, given that the only negative of using the smallest possible increment size is computational cost, which is negligible here.

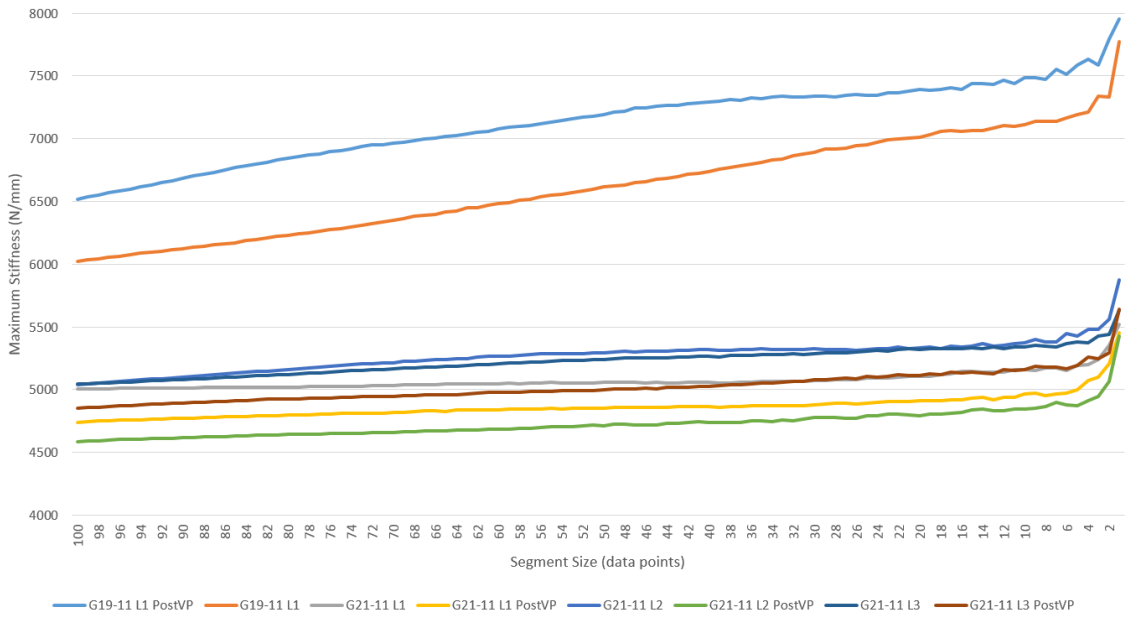

Figure 1.2.1: The effect of reducing the segment size on the maximum stiffness reported from four human vertebrae loaded to 2000 N pre and post augmentation. Using an increment size of 1 data point (0.0017 mm) and segment sizes of 100 to 1 data point (0.17 mm to 0.0017 mm).

Using an increment size of 1 data points width, as shown in Figure 1.2.1 shows a smaller variation across the range of segment sizes compared to using 20 points in Figure 1.2.2. The effect of both

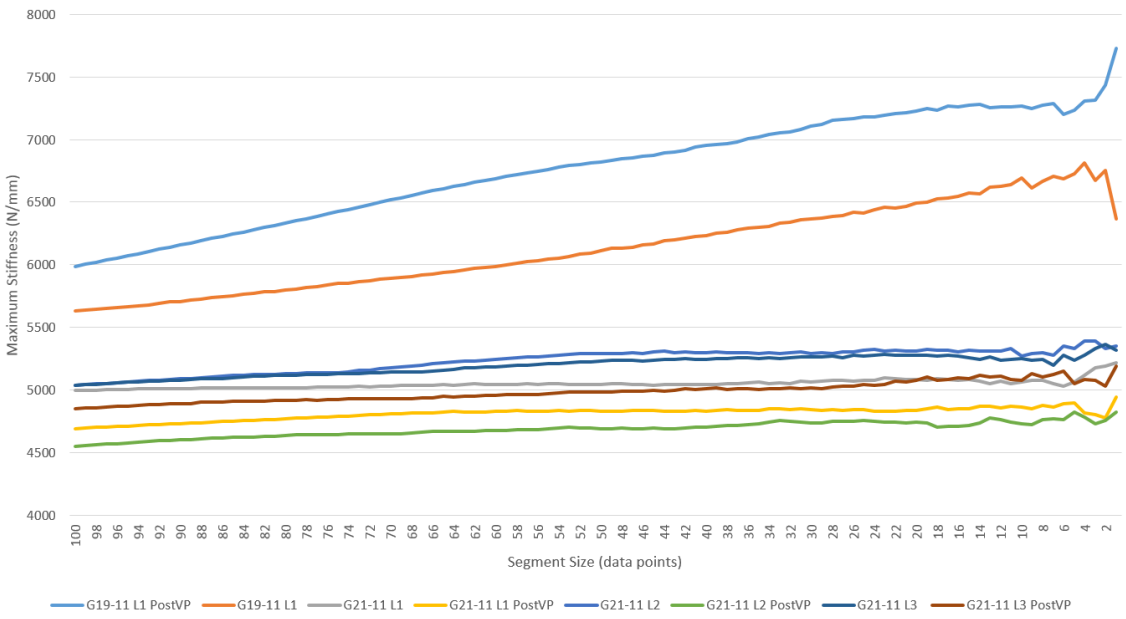

Figure 1.2.2: The effect of reducing the segment size on the maximum stiffness reported from four human vertebrae loaded to 2000 N pre and post augmentation. Using an increment size of 20 data points (0.0037 mm) and segment sizes of 100 to 1 data point (0.17 mm to 0.0017 mm).

segment size and increment size is especially evident for the two G19-11 L1 vertebrae both intact and post augmentation where the stiffness continues to increase until the end of the test at 2000 N. Meaning that there is a much smaller linear region for these two specimens, hence requiring a smaller segment size to measure the largest gradient.

Choosing values for the segment size to use moving forwards becomes difficult given the large effect it can have on the measured maximum stiffness (a range of over 1000 N/mm in the case the two G19-11 L1 tests). The segment size needs to be small enough to capture the maximum stiffness while avoiding the noise when using a segment size below 18 data points. Hence, a value of 20 data points was chosen, a value that avoids the noise while being on the plateau of the lines.

1.2.2.2 Repeated Loading

Given the nature of the test, attempting to limit damage to the vertebrae, especially during their initial intact load, the ability to derive errors becomes difficult especially from a single load. To attempt to understand this error four vertebrae having undergone augmentation were tested three more times in an iterative fashion, removing each from the load testing machine, testing the next specimen in the set and repeating. Removing the vertebrae from their steel housing (instead of three tests while seated in the steel housing) allowed the error in loading position and setup to be tested along with repeated loading of the vertebrae to be tested.

The results of repeated loading can be seen in Figure 1.2.3. All four specimens show a reduced stiffness for the repeated loads following the initial load, for which there are a few possible reasons. One possibility for the reduction in stiffness is that it is a consequence of the freeze thaw cycle that occurred between these tests. The second possibility is that the vertebrae were still partially frozen while the testing took place. Finally, it could be due to damage being caused during the initial load to 2000 N, shown in Figures 1.2.4 to 1.2.7 it is possible to see slight failure in the three G21-11 vertebrae, although failure cannot be seen in the G19-11 L1 vertebrae. The

frozen bar in Figure 1.2.3 shows how the stiffness increases when the vertebrae are completely frozen, potentially helping to explain the drop in stiffness found in the repeats. Further tests will be carried out with three more repeats following another freeze thaw cycle to attempt to answer this.

The iterative reduction in stiffness for the G21-11 L2 vertebrae can be explained as damage being caused after each iteration. This can be seen in Figure 1.2.6, with the three repeats each showing a yielding before the 1600 N limit and a smaller maximum load and stiffness after each repeat.

Figures 1.2.4 through 1.2.7 show the data for the loading, from which the maximum stiffness values are found. This excludes the initial cyclic loading, starts the loading at 50 N and displacement at 0 mm.

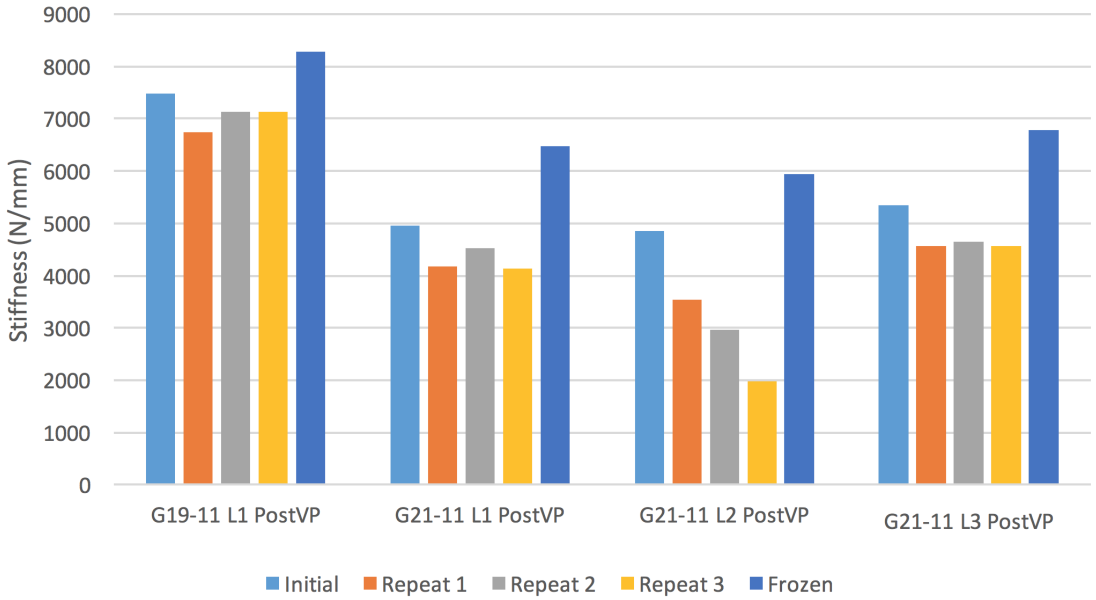

Figure 1.2.3: The stiffness of four augmented vertebral specimens over the course of an initial load, three repeated loads and a load while frozen. The intact specimen was loaded until 2000 N while the remaining four were loaded until 1600 N.

1.2.3 Vertebroplasty

Despite the development of methods for the augmentation of bovine tail vertebrae, the methods for augmenting human vertebrae were altered due to the different geometry and density. The human vertebrae, being much less dense, did not require the vertebroplasty needle to be inserted with the aid of a mallet. Instead the needle could be pushed by hand through the cortical shell and into the vertebral body.

An additional difference was the approach with the needle, instead of entering the vertebrae through their pedicles an oblique approach was adopted. This was due to variation in pedicle diameter between the L1 - L5 lumbar levels and therefore the potential to damage the region and its load sharing capabilities. The oblique approach therefore avoided creating this damage to the pedicle-canal region, especially for the vertebrae with narrower pedicles and instead created much less damage to the vertebral body.

A final difference to the needle insertion methods was a change to the needle. Here, a side

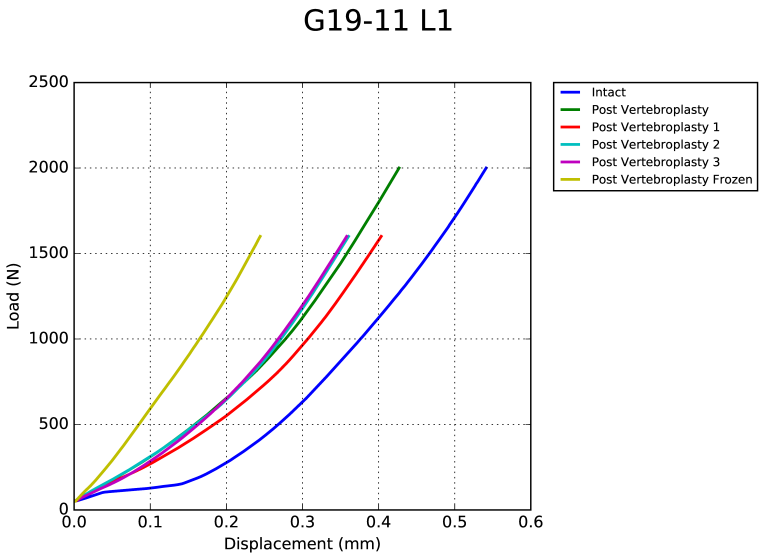

Figure 1.2.4: The load - displacement results for the G19-11 L1 vertebra. Showing results of the intact load and post augmentation load up to 2000 N and the repeats and frozen load up to 1600 N.

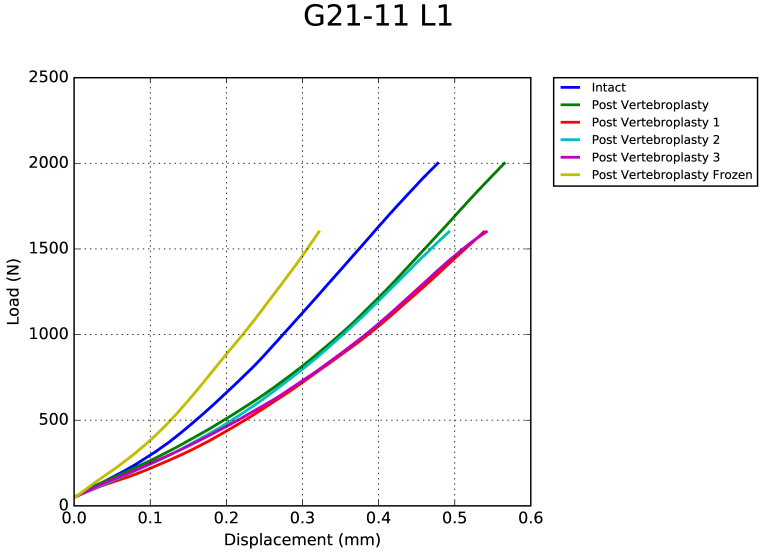

Figure 1.2.5: The load - displacement results for the G21-11 L1 vertebra. Showing results of the intact load and post augmentation load up to 2000 N and the repeats and frozen load up to 1600 N.

opening needle was used, allowing the cement to be directed into the anterior-centre region of the vertebral body as opposed to directly out of the needle end.

Quantity?

1.2.4 Vertebrae Characteristics

Identifying the different characteristics for the set of lumbar vertebrae has importance in understanding trends and relationships between the experimental and computational results. For example a larger degree of anisotropy and hence more directionality aligned trabeculae would

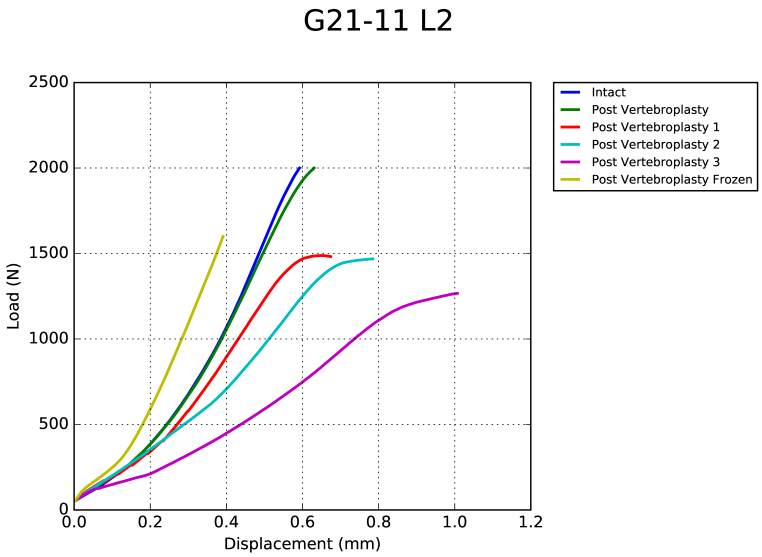

Figure 1.2.6: The load - displacement results for the G21-11 L2 vertebra. Showing results of the intact load and post augmentation load up to 2000 N and the repeats and frozen load up to 1600 N.

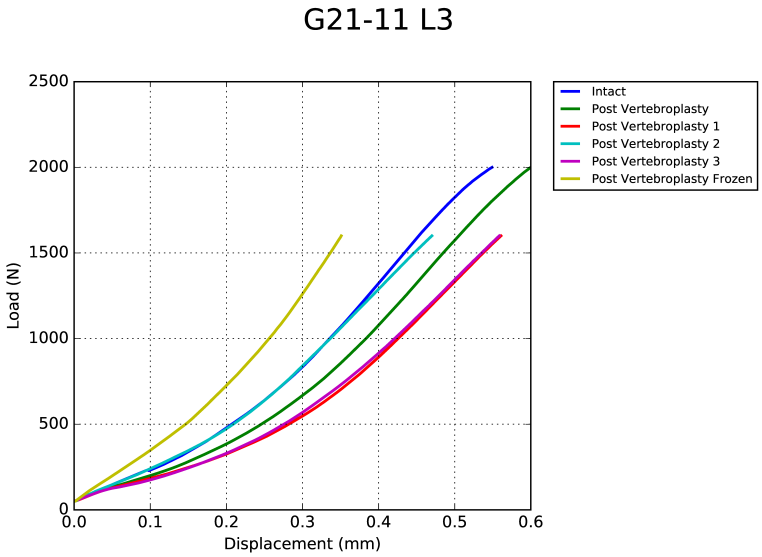

Figure 1.2.7: The load - displacement results for the G21-11 L3 vertebra. Showing results of the intact load and post augmentation load up to 2000 N and the repeats and frozen load up to 1600 N.

potentially give a more experimentally stiff vertebra, despite otherwise similar characteristics. Given that much of the vertebral characteristics depend on the trabecular structure it is important to understand how this varies between specimens. Furthermore, any calculations originating from a description of the trabecular structure require a correct threshold to be applied to the μCT scan. This threshold describes the limit of the trabecular bone and hence the start of either marrow or empty space. To enable a fair comparison between vertebrae a region of interest was selected from the vertebral body. Given the large variation in cortical shell thickness, along with certain vertebrae containing large osteophytes and other extra bone growth, the region of interest (ROI) was selected to be the largest cylinder that could fit within the vertebral body while not capturing any of the cortical shell.

1.2.4.1 Histograms

In order to understand the spread of brightness' from the set of lumbar the histograms of the ROIs were plotted (Figure 1.2.8).

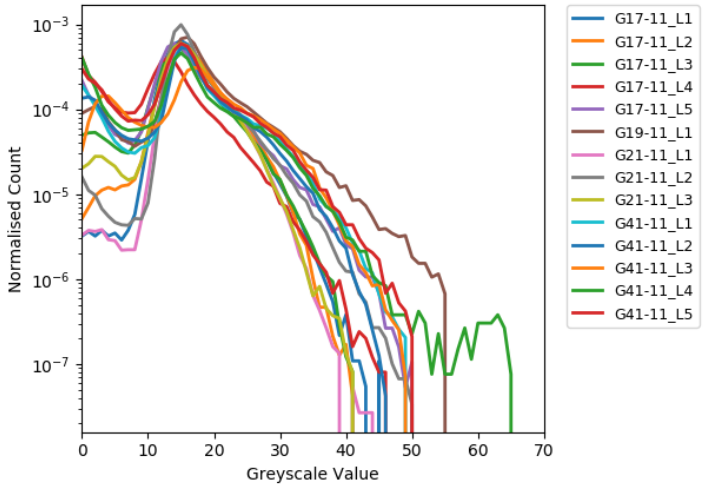

Figure 1.2.8: The normalised (with respect to the volume of the ROI) histogram data for the 14 lumbar vertebrae.

The lower greyscale values represent the empty space within the ROI which translates to regions where the bone marrow has exited the region, most likely during the freeze thaw cycles. The peak in the histogram at an approximate greyscale value of 16 is due to the bone marrow. The remaining portion of the histogram represents bone, where variation is due to the differences in the mineral content of the bone, with more mineralised bone appearing brighter on μCT scans. The specimens ROIs that contain the brighter values are those that contain osteophytes that contain more dense bone than the other cortical shell, for example G19-11 L1.

1.2.4.2 Threshold Optimisation

The full resolution scan is imported into imageJ where the threshold optimisation is carried out. The BoneJ plugin for imageJ is used for all of the trabecular structure metrics, with the optimise threshold tool being the focus here. This tool is run on the region of interest using the default settings for the connectivity options seen in Table 1.2.1. This chooses a threshold based on the peak in a connectivity against threshold plot and reports that value. These values can be seen in Table 1.2.2, showing considerable across the range of vertebrae. However, the differences in these suggested thresholds can grouped with the spine, for example: the G17 spine has a range between 15 to 17, while the G41 spine has an range between 18 to 20. This promotes the idea that these differences are due to the bone mineralisation of the bone, especially given that the G17 spine is from a Female and G41 from a male.

However, given that the chosen value for the threshold will directly impact the reported metrics, a consistent value has been chosen of 18. Using lower or higher values for the threshold usually results in the trabeculae being described as thicker or thinner respectively. Hence, the difference in the mineralisation between specimens will still be captured when using a fixed threshold, given that the binary image will be down sampled before material properties are acquired. The results in Table 1.2.3 show the BV / TV data and degree of anisotropy values for the 14 specimens

using the fixed threshold of 18. Similar trends to what could be seen from the optimise threshold results can be seen in the BV/TV data, with grouping between the spines evident.

Table 1.2.1: Settings used for the ImageJ plugin, BoneJ: Optimise Threshold.

Options	Values
Tests	11
Range	0.2
Subvolume Size	256
Erosian Cycles	0
Dilation Cycles	0

Table 1.2.2: The suggested threshold from the optimise threshold BoneJ tool for the 14 lumbar vertebrae in the set.

Specimen	Suggested Threshold
G17-11_L1	17
G17-11_L2	16
G17-11_L3	16
G17-11_L4	15
G17-11_L5	16
G19-11_L1	23
G21-11_L1	18
G21-11_L2	19
G21-11_L3	19
G41-11_L1	20
G41-11_L2	19
G41-11_L3	18
G41-11_L4	19
G41-11_L5	18

Table 1.2.3: BV/TV and degree of anisotropy (DA) values found using the ImageJ plugin BoneJ tools Volume Fraction and Annisotropy respectively using a threshold of 18.

Specimen	BV/TV	DA
G17-11_L1	0.174	0.387
G17-11_L2	0.17	0.364
G17-11_L3	0.137	0.359
G17-11_L4	0.127	0.418
G17-11_L5	0.187	0.341
G19-11_L1	0.391	0.199
G21-11_L1	0.255	0.327
G21-11_L2	0.267	0.231
G21-11_L3	0.281	0.301
G41-11_L1	0.257	0.239
G41-11_L2	0.241	0.338
G41-11_L3	0.244	0.348
G41-11_L4	0.247	0.371
G41-11_L5	0.249	0.186

1.2.5 Modelling

Given the aims of the project - to include the models generated here into a larger set of vertebral models for use in statistical shape modelling, it is useful to model the vertebrae in a scanner independent method. A method for doing this (BV/TV modelling method) uses a full resolution scan with the bone regions segmented using a threshold. This full resolution segmented scan is then downsampled to voxels with edge length of 1 mm, meaning that each voxel has a greyscale value proportional to the BV/TV value for the region captured by that voxel. Areas that contain more bone will therefore have a higher greyscale value. This method is purely dependant on the threshold selected defining the bone and hence, given that threshold values can be repeatedly and correctly selected, is scanner independent.

1.2.5.1 BV/TV Modelling Method

The method follows that found in a study by Robson Brown et al. [59] with a few minor changes. The scans are converted into a stack of TIFF files using an in house Matlab script, which in addition reduces the 16 bit file to 8 bit images.

The set of vertebral specimens were split at this stage into two sets, allowing an understanding of the effect of specimen specific thresholds for the vertebral models, these sets used a threshold of 21 for the Uniform test and their BoneJ predicted value for the Different Threshold Set. Following the application of the threshold (creating a binary image stack) a Gaussian filter with $\sigma_{x,y,z} = 1$ was applied in order to remove speckling found surrounding the end-caps. The two stacks of images are then imported into ScanIP; carried out by opening one stack of images (the original stack) and then importing a second background (the binary image stack). Both backgrounds are downsampled to voxel sizes of 1 mm^3, with the (originally) binary stack being used to create the mask for the vertebrae and the original stack being used for the end-caps. Greyscale material properties for the vertebral mask are taken from the binary stack, while the remainder of the methods follow the same process as the original method.

1.2.5.2 Predicting Vertebral Yield Point

1.2.5.3 Load Position Sensitivity

1.2.5.4 Modelling Augmentation

Artificial brightening of regions surrounding the internal cement, specifically concentrated areas of barium sulphate and the artefacts this can cause affect the material properties that are applied to the material. To bypass this effect the two models, intact and post-augmentation models can be registered - translating them into the same spacial location. This allows the cement to be defined, masked and modelled based on the post-augmentation scan and the remaining vertebra to be defined from the intact scan, the same background used for the intact models. While the shape of the vertebra may have been changed over the course of its two loads, this change is less than what can be seen at 1 mm resolution. Additionally regions that have experienced damage through the insertion of the needle, yet do not contain cement will also be neglected using this method. However, the same justification can be made, where this is unlikely to have any affect at 1 mm resolution.

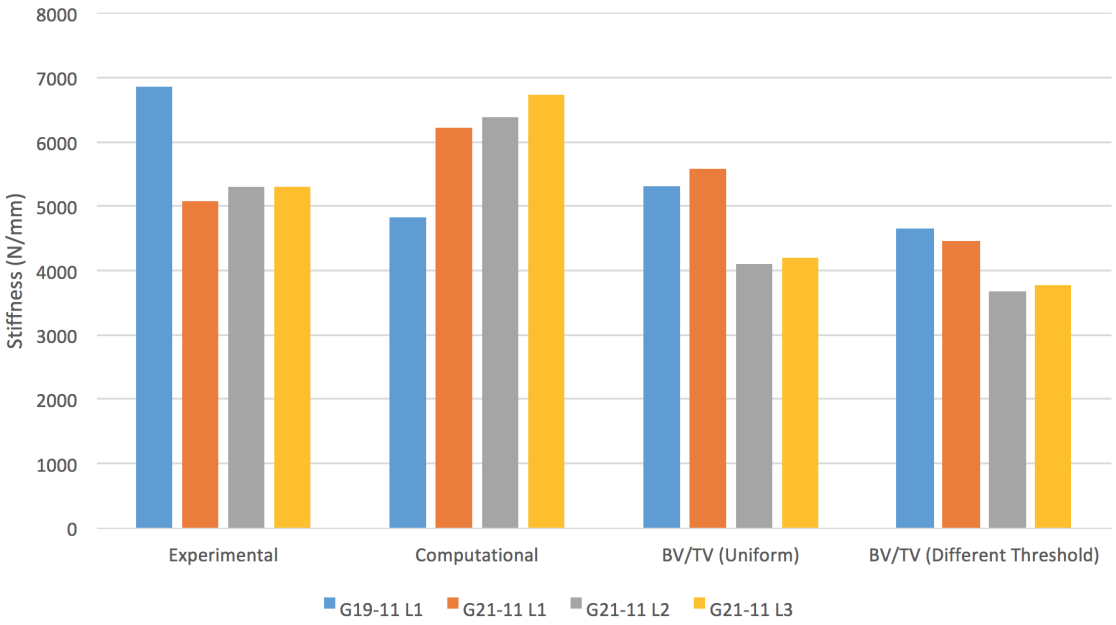

Figure 1.2.9: The stiffness results of three different FE methods for four intact human vertebrae compared to the experimental stiffness results. Interest should be drawn to the ratio between specimen models rather than the values themselves, given that the conversion factors between greyscale values and Young's modulus have not been optimised at this stage. Results show the difference between the currently used method of modelling the vertebrae and the BV/TV based methods (both with uniform thresholds and different thresholds for each specimen).

1.3 Results

1.4 Discussion

1.5 Conclusion

Bibliography

[1] Henry. Gray. *Anatomy of the human body.* 20th ed., edition, 1918.

[2] F. Magerl, M. Aebi, S. D. Gertzbein, J. Harms, and S. Nazarian. A comprehensive classification of thoracic and lumbar injuries. *Eur. Spine J.*, 3(4):184–201, aug 1994.

[3] J. Aerssens, J., Boonen, S., Lowet, G., Dequekker. Interspecies Differences in Bone Composition , Density , and Quality : Potential Implications for in Vivo Bone Research. *Endocrinology*, 139(2):663–670, 1998.

[4] Jenni M. Buckley. Sensitivity of Vertebral Compressive Strength to Endplate Loading Distribution. *J. Biomech. Eng.*, 128(5):641, 2006.

[5] Stephen M Belkoff, John M Mathis, and Louis E Jasper. The Biomechanics of Vertebroplasty. *Spine (Phila. Pa. 1976).*, 26(14):1537–1541, 2001.

[6] M a Liebschner, W S Rosenberg, and T M Keaveny. Effects of bone cement volume and distribution on vertebral stiffness after vertebroplasty. *Spine (Phila. Pa. 1976).*, 26(14):1547–1554, 2001.

[7] Lorenzo Grassi, Enrico Schileo, Christelle Boichon, Marco Viceconti, and Fulvia Taddei. Comprehensive evaluation of PCA-based finite element modelling of the human femur. *Med. Eng. Phys.*, 36(10):1246–52, oct 2014.

[8] Michael A. Adams and Patricia Dolan. Spine biomechanics. *J. Biomech.*, 38(10):1972–1983, oct 2005.

[9] T.D. Stewart and R.M. Hall. (iv) Basic biomechanics of human joints: Hips, knees and the spine. *Curr. Orthop.*, 20(1):23–31, feb 2006.

[10] Narayan Yoganandan, Frank a Pintar, Brian D Stemper, Jamie L Baisden, Recyi Aktay, Barry S Shender, Glenn Paskoff, and Purushottam Laud. Trabecular bone density of male human cervical and lumbar vertebrae. *Bone*, 39(2):336–44, aug 2006.

[11] Manohar M. Panjabi, Koichiro Takata, Vijay Goel, Dale Federico, Thomas Oxland, Joanne Duranceau, and Martin Krag. Thoracic Human Vertebrae Quantitative Three-Dimensional Anatomy. *Spine (Phila. Pa. 1976).*, 16(8):888–901, 1991.

[12] Panjabi M. Manohar, Vijay Goel, Thomas Oxland, Koichiro Takata, Joanne Duranceau, Martin Krag, and Mark Price. Human lumbar vertebrae: quantitative three-dimensional anatomy, 1992.

[13] F Denis. The three column spine and its significance in the classification of acute thoracolumbar spinal injuries. *Spine (Phila Pa 1976)*, 8(8):817–831, 1983.

[14] J M Mathis, J D Barr, S M Belkoff, M S Barr, M E Jensen, and H Deramond. Percutaneous vertebroplasty: a developing standard of care for vertebral compression fractures. *AJNR. Am. J. Neuroradiol.*, 22(February):373–381, feb 2001.

[15] Case Studies, From The, and Mayo Clinic. Vertebral Compression Fractures in Elderly Osteoporosis Patients Receiving Glucocorticoid Intra-articular Injections. *Am. Fam. Physician*, 6(3):206–211, 2006.

[16] L J Melton III and David F Kallmes. Epidemiology of vertebral fractures: implications for vertebral augmentation. *Acad. Radiol.*, 13(5):538–45, may 2006.

[17] C Cooper, E J Atkinson, W M O'Fallon, and L J Melton. Incidence of clinically diagnosed vertebral fractures: a population-based study in Rochester, Minnesota, 1985-1989. *J. Bone Miner. Res.*, 7(2):221–227, feb 1992.

[18] Fernando Burstein, Steven Cohen, Roger Hudgins, William Boydston, and Catherine Simms. The Use of Hydroxyapatite Cement in Secondary Craniofacial Reconstruction. *Craniofacial Reconstr.*, 104(5):1270–1275, jan 1987.

[19] C. Cooper, T. O'Neill, and A. Silman. The epidemiology of vertebral fractures. *Bone*, 14:89–97, jan 1993.

[20] Terrence H Diamond, Carl Bryant, Lois Browne, and William a Clark. Clinical outcomes after acute osteoporotic vertebral fractures: a 2-year non-randomised trial comparing percutaneous vertebroplasty with conservative therapy. *Med. J. Aust.*, 184(3):113–7, 2006.

[21] M. Moro, a. T. Hecker, M. L. Bouxsein, and E. R. Myers. Failure load of thoracic vertebrae correlates with lumbar bone mineral density measured by DXA. *Calcif. Tissue Int.*, 56(3):206–209, mar 1995.

[22] A. A. BOOKMAN. *Musculoskeletal Imaging*, volume 38. Elsevier Health Sciences, 2011.

[23] Rachelle Buchbinder, Richard H Osborne, Peter R Ebeling, John D Wark, Peter Mitchell, Chris Wriedt, Stephen Graves, Margaret P Staples, and Bridie Murphy. A randomized trial of vertebroplasty for painful osteoporotic vertebral fractures. *N. Engl. J. Med.*, 361(6):557–568, 2009.

[24] David F Kallmes, Bryan A Comstock, Patrick J Heagerty, Judith A Turner, David J Wilson, Terry H Diamond, Richard Edwards, Leigh A Gray, Lydia Stout, Sara Owen, William Hollingworth, Basavaraj Ghdoke, Deborah J Annesley-Williams, Stuart H Ralston, and Jeffrey G Jarvik. A randomized trial of vertebroplasty for osteoporotic spinal fractures. *N. Engl. J. Med.*, 361(6):569–79, 2009.

[25] Stephen M Belkoff, John M Mathis, and Louis E Jasper. Ex vivo biomechanical comparison of hydroxyapatite and polymethylmethacrylate cements for use with vertebroplasty. *AJNR. Am. J. Neuroradiol.*, 23(10):1647–51, 2002.

[26] Paul A Hulme, Jörg Krebs, Stephen J Ferguson, and Ulrich Berlemann. Vertebroplasty and kyphoplasty: a systematic review of 69 clinical studies. *Spine (Phila. Pa. 1976).*, 31(17):1983–2001, aug 2006.

[27] SPJ Muijs. Treatment of painful osteoporotic vertebral compression fractures: A Brief Review of the Evidence for Percutaneous Vertebroplasty. *J. Bone Jt. ...*, 2011.

[28] B Jay and SH Ahn. Vertebroplasty. *Semin. Intervent. Radiol.*, 2013.

[29] P J Atkinson. Variation in trabecular structure of vertebrae with age. *Calcif. Tissue Res.*, 1(1):24–32, 1967.

[30] a M Parfitt. Age-related structural changes in trabecular and cortical bone: cellular mechanisms and biomechanical consequences. *Calcif. Tissue Int.*, 36 Suppl 1(1):S123–S128, 1984.

[31] Je Aaron, Pa Shore, Rc Shore, M Beneton, and Ja Kanis. Trabecular architecture in woman and men of similar bone mass with and without vertebral fracture: II. Three-dimensional histology. *Bone*, 27(2):277–282, 2000.

[32] P. a. Hulme, S. K. Boyd, and S. J. Ferguson. Regional variation in vertebral bone morphology and its contribution to vertebral fracture strength. *Bone*, 41(6):946–957, 2007.

[33] L Mosekilde, L Mosekilde, and C C Danielsen. Biomechanical competence of vertebral trabecular bone in relation to ash density and age in normal individuals. *Bone*, 8(2):79–85, 1987.

[34] Tony S Keller. Predicting the Compressive Mechanical Behavior of Bone. *J. Biomech.*, 27(9):1159–1168, 1994.

[35] Tor Hildebrand and Peter Rüegsegger. Quantification of Bone Microarchitecture with the Structure Model Index. *Comput. Methods Biomech. Biomed. Engin.*, 1(1):15–23, 1997.

[36] Jesper Skovhus Thomsen, E N Ebbesen, and Li I Mosekilde. Zone-dependent changes in human vertebral trabecular bone: clinical implications. *Bone*, 30(5):664–9, 2002.

[37] Ebbe N Ebbesen, Jesper S Thomsen, Henning Beck-Nielsen, Hans J Nepper-Rasmussen, and Lis Mosekilde. Age-and Gender-Related Differences in Vertebral Bone Mass, Density, and Strength. *J. Bone Miner. Res.*, 14(8):1394–1403, 1999.

[38] H-J Wilke, A Kettler, and L E Claes. Are sheep spines a valid biomechanical model for human spines? *Spine (Phila. Pa. 1976).*, 22(20):2365–2374, 1997.

[39] Frank Kandziora, Robert Pflugmacher, Matti Scholz, Klaus Schnake, Martin Lucke, Ralf Schröder, and Thomas Mittlmeier. Comparison Between Sheep and Human Cervical Spines An Anatomic, Radiographic, Bone Mineral Density, and Biomechanical Study. *Spine (Phila. Pa. 1976).*, 26(9):1028–1037, 2001.

[40] Hans-Joachim Wilke, Annette Kettler, and Karl Howard Wenger. Anatomy of the Sheep Spine and Its Comparison to the Human Spine. *Anat. Rec.*, 247(4):542–555, 1997.

[41] V N Wijayathunga, a C Jones, R J Oakland, N R Furtado, R M Hall, and R K Wilcox. Development of specimen-specific finite element models of human vertebrae for the analysis of vertebroplasty. *Proc. Inst. Mech. Eng. H.*, 222(2):221–228, feb 2008.

[42] Sami M Tarsuslugil, Rochelle M O'Hara, Nicholas J Dunne, Fraser J Buchanan, John F Orr, David C Barton, and Ruth K Wilcox. Development of calcium phosphate cement for the augmentation of traumatically fractured porcine specimens using vertebroplasty. *J. Biomech.*, 46(4):711–5, 2013.

[43] Navin Furtado, Robert J Oakland, Ruth K Wilcox, and Richard M Hall. A biomechanical investigation of vertebroplasty in osteoporotic compression fractures and in prophylactic vertebral reinforcement. *Spine (Phila. Pa. 1976).*, 32(17):E480–E487, 2007.

[44] R K Wilcox, D J Allen, R M Hall, D Limb, D C Barton, and R a Dickson. A dynamic investigation of the burst fracture process using a combined experimental and finite element approach. *Eur. Spine J.*, 13(6):481–8, 2004.

[45] GS Gurwitz, JM Dawson, and MJ McNamara. Biomechanical analysis of three surgical approaches for lumbar burst fractures using short-segment instrumentation. *Spine (Phila. Pa. 1976).*, 1993.

[46] Dheera Ananthakrishnan, Sigurd Berven, Vedat Deviren, Kevin Cheng, Jeffrey C Lotz, Zheng Xu, and Christian M Puttlitz. The effect on anterior column loading due to different vertebral augmentation techniques. *Clin. Biomech. (Bristol, Avon)*, 20(1):25–31, 2005.

[47] U Berlemann, S J Ferguson, L P Nolte, and P F Heini. Adjacent vertebral failure after vertebroplasty. A biomechanical investigation. *J. Bone Joint Surg. Br.*, 84(5):748–752, 2002.

[48] Spiros G. Pneumaticos, Georgios K. Triantafyllopoulos, Dimitrios S. Evangelopoulos, John a. Hipp, and Michael H. Heggeness. Effect of vertebroplasty on the compressive strength of vertebral bodies. *Spine J.*, 13(12):1921–1927, 2013.

[49] John D. Barr, Michelle S. Barr, Thomas J. Lemley, and Richard M. McCann. Percutaneous Vertebroplasty for Pain Relief and Spinal Stabilization. *Spine (Phila. Pa. 1976).*, 25(8):923–928, apr 2000.

[50] A G Tohmeh, J M Mathis, D C Fenton, A M Levine, and S M Belkoff. Biomechanical efficacy of uni- vs. bi-pedicular vertebroplasty for the treatment of osteoporotic compression fractures. *Trans. Orthop. Res. Soc.*, 24(17):177, 1999.

[51] Stephen M Belkoff, John M Mathis, and Erik M Erbe. Biomechanical Evaluation of a New Bone Cement for Use in Vertebroplasty. *Spine (Phila. Pa. 1976).*, 25(9):1061–1064, 2000.

[52] Kathryn B Higgins, David R Sindall, Alberto M Cuitino, and Noshir a Langrana. Biomechanical alterations in intact osteoporotic spine due to synthetic augmentation: finite element investigation. *J. Biomech. Eng.*, 129(4):575–85, 2007.

[53] Jove Graham, Michael Ries, and Lisa Pruitt. Effect of bone porosity on the mechanical integrity of the bone-cement interface. *J. Bone Joint Surg. Am.*, 85-A(10):1901–1908, 2003.

[54] S Belkoff, H Deramond, J Mathis, and L Jasper. Vertebroplasty: the biomechanical effect of cement volume. *Trans Orthop Res Soc*, 46:356, 2000.

[55] S J Lee, B J Jun, G R Tack, S Y Lee, and K C Shin. Prediction and assessment of optimal volume for PMMA injection in percutaneous vertebroplasty using image and biomechanical analyses. In *Trans. Annu. Meet. Res. Soc.*, page 786, 2002.

[56] Alison C. Jones and Ruth K. Wilcox. Finite element analysis of the spine: Towards a framework of verification, validation and sensitivity analysis. *Med. Eng. Phys.*, 30(10):1287–1304, dec 2008.

[57] Marco Viceconti, Sigbjorn Olsen, Lutz P. Nolte, and Kim Burton. Extracting clinically relevant data from finite element simulations. *Clin. Biomech.*, 20(5):451–454, jun 2005.

[58] Marlène Mengoni, Sebastien N.F. Sikora, Vinciane D'Otreppe, Ruth K. Wilcox, and Alison C. Jones. In-silico models of trabecular bone: a sensitivity analysis perspective. 2014.

[59] K Robson Brown, S Tarsuslugil, V N Wijayathunga, and R K Wilcox. Comparative finite-element analysis: a single computational modelling method can estimate the mechanical properties of porcine and human vertebrae. *J. R. Soc. Interface*, 11(95):20140186, jun 2014.

[60] Yan Chevalier, Dieter Pahr, and Philippe K. Zysset. The Role of Cortical Shell and Trabecular Fabric in Finite Element Analysis of the Human Vertebral Body. *J. Biomech. Eng.*, 131(11):111003, nov 2009.

[61] Senthil K. Eswaran, Atul Gupta, and Tony M. Keaveny. Locations of bone tissue at high risk of initial failure during compressive loading of the human vertebral body. *Bone*, 41(4):733–739, oct 2007.

[62] Michael Kinzl, Lorin M. Benneker, Andreas Boger, Philippe K. Zysset, and Dieter H. Pahr. The effect of standard and low-modulus cement augmentation on the stiffness, strength, and endplate pressure distribution in vertebroplasty. *Eur. Spine J.*, 21(5):920–929, may 2012.

[63] G M Treece, R W Prager, and A H Gee. Regularised marching tetrahedra : improved iso-surface extraction. *Comput. Graph.*, 23:583–598, 1999.

[64] Senthil K Eswaran, Atul Gupta, Mark F Adams, and Tony M Keaveny. Cortical and Trabecular Load Sharing in the Human Vertebral Body. *J. Bone Miner. Res.*, 21(2):307–314, nov 2005.

[65] H Ritzel, M Amling, M Pösl, M Hahn, and G Delling. The thickness of human vertebral cortical bone and its changes in aging and osteoporosis: a histomorphometric analysis of the complete spinal column from thirty-seven autopsy specimens. *J. Bone Miner. Res.*, 12(1):89–95, 1997.

[66] Dieter H. Pahr and Philippe K. Zysset. A comparison of enhanced continuum FE with micro FE models of human vertebral bodies. *J. Biomech.*, 42(4):455–462, mar 2009.

[67] G. Baroud, J. Nemes, P. Heini, and T. Steffen. Load shift of the intervertebral disc after a vertebroplasty: A finite-element study. *Eur. Spine J.*, 12(4):421–426, aug 2003.

[68] Anne Polikeit, Lutz Peter Nolte, and Stephen J Ferguson. The effect of cement augmentation on the load transfer in an osteoporotic functional spinal unit: finite-element analysis. *Spine (Phila. Pa. 1976).*, 28(10):991–996, 2003.

[69] Yan Chevalier, Dieter Pahr, Mathieu Charlebois, Paul Heini, Erich Schneider, and Philippe Zysset. Cement Distribution, Volume, and Compliance in Vertebroplasty. *Spine (Phila. Pa. 1976).*, 33(16):1722–1730, 2008.

[70] Y Zhao, K a Robson Brown, Z M Jin, and R K Wilcox. Trabecular level analysis of bone cement augmentation: a comparative experimental and finite element study. *Ann. Biomed. Eng.*, 40(10):2168–76, oct 2012.

[71] Gianluca Tozzi, Qing-Hang Zhang, and Jie Tong. 3D real-time micromechanical compressive behaviour of bone - cement interface: Experimental and finite element studies. *J. Biomech.*, 45(2):356–363, jan 2012.

[72] Dennis Janssen, Kenneth a. Mann, and Nico Verdonschot. Micro-mechanical modeling of the cement-bone interface: The effect of friction, morphology and material properties on the micromechanical response. *J. Biomech.*, 41(15):3158–3163, nov 2008.

[73] M. Kinzl, a. Boger, P. K. Zysset, and D. H. Pahr. The mechanical behavior of PMMA/bone specimens extracted from augmented vertebrae: A numerical study of interface properties, PMMA shrinkage and trabecular bone damage. *J. Biomech.*, 45(8):1478–1484, may 2012.

[74] Mr Sebastien Sikora. Experimental and Computational Study of the Behaviour of Trabecular Bone-Cement Interfaces. pages 196–244, 2013.

[75] Sami P Väänänen, Lorenzo Grassi, Gunnar Flivik, Jukka S Jurvelin, and Hanna Isaksson. Generation of 3D shape, density, cortical thickness and finite element mesh of proximal femur from a DXA image. *Med. Image Anal.*, 24(1):125–34, aug 2015.

[76] C Rao and CK Fitzpatrick. A statistical finite element model of the knee accounting for shape and alignment variability. *Med. Eng. ...*, 2013.

[77] CK Fitzpatrick, MA Baldwin, and PJ Laz. Development of a statistical shape model of the patellofemoral joint for investigating relationships between shape and function. *J. ...*, 2011.

[78] Stephen M. Belkoff, Janis C. Sanders, and Louis E. Jasper. The effect of the monomer-to-powder ratio on the material properties of acrylic bone cement. *J. Biomed. Mater. Res.*, 63(4):396–399, 2002.

[79] L. E. Jasper, H. Deramond, J. M. Mathis, and S. M. Belkoff. The effect of monomer-to-powder ratio on the material properties of cranioplastic. *Bone*, 25(SUPPL. 1):27–29, 1999.

[80] A C Jones and R K Wilcox. Assessment of factors influencing finite element vertebral model predictions. *J Biomech Eng*, 129(6):898–903, 2007.

[81] Amos Race, Kenneth A. Mann, and Avram A. Edidin. Mechanics of bone/PMMA composite structures: An in vitro study of human vertebrae. *J. Biomech.*, 40(5):1002–1010, 2007.